Available online at www.sciencedirect.com

ScienceDirect

Procedia Structural Integrity 39 (2022) 403–408

Structural Integrity Procedia

www.elsevier.com/locate/procedia

7th International Conference on Crack Paths

Effect of variable amplitude block loading on fatigue crack growth

D.M. Neto[a], M.F. Borges[a], J.M. Silva[a], F.V. Antunes[a,*]

[a]*Univ Coimbra, Centre for Mechanical Engineering, Materials and Processes (CEMMPRE), Department of Mechanical Engineering, Rua Luís Reis Santos, 3030-788 Coimbra, Portugal*

Abstract

The objective is to study the effect of load blocks on fatigue crack propagation. To carry out this study, the finite element program DD3IMP will be used, with the fatigue crack propagation being controlled by the value of the plastic deformation at the end of the crack. The material used was the Ti6Al4V alloy obtained by the selective laser fusion manufacturing process. Regarding the studied load patterns, two types of High-Low load blocks and two types of Low-High load blocks were studied. A plane stress state was always considered and the influence of the contact between the crack flanks on the predicted FCG rate is highlighted by removing numerically the contact conditions. The transient behavior observed between loading blocks of different amplitude is strongly reduced or vanishes when the contact is neglected. For load blocks with high values of stress ratio, the predicted FCG rate in steady state regime is approximately the same considering or neglecting the contact of the crack flanks. On the other hand, for low values of stress ratio, the predicted FCG rate is lower when the contact of the crack flanks is considered, which is related with crack closure level.

Keywords: Fatigue crack growth; Load blocks; Crack closure; Ti6Al4V

1. Introduction

Real components and structures are typically submitted to complex loading patterns. Design against fatigue based on damage tolerance approach requires the knowledge of fatigue crack growth (FCG) rate. However, there is a great complexity associated with real load patterns, and it is important to start studying simpler patterns for a progressive

* Corresponding author. Tel.: +351 239 790 700; fax: +351 239 790 701.
E-mail address: fernando.ventura@dem.uc.pt

10.1016/j.prostr.2022.03.109

understanding of the underlying mechanisms. In a strategy of increasing complexity, it is natural to consider in a first approach the study of overloads and load blocks. Different mechanisms have been proposed to explain the effect of variable amplitude loading, namely crack tip blunting (Christensen, 1959), residual stresses (Schijve, 1962), strain hardening (Jones, 1973), crack branching (Suresh, 1983) and plasticity induced crack closure (Neto, 2021). In a previous work (Neto, 2021) it was found that the transient behavior following overloads in only linked to crack closure phenomenon. It is important to verify if this holds in the case of load blocks.

Therefore, this research studies the transient effects observed in Low-High and High-Low load sequences. A numerical approached based on cumulative plastic strain was followed to predict FCG in CT specimens. Models with and without contact of crack flanks were considered to isolate the effect of crack closure phenomenon.

2. Numerical model

The numerical simulations of FCG were performed using the in-house finite element code DD3IMP (Menezes, 2000). Different block loadings (mode I) are applied to Compact Tension (CT) specimens, whose geometry and dimensions are according to ASTM E647-15 (2015). The normalized size of the CT specimen is W=36 mm, presenting 16 mm of the initial crack length. Due to the symmetry conditions, only the upper part of the CT specimen was simulated under plane stress conditions. The contact of the crack flanks is simulated by placing a rigid surface at the symmetry plane, which can be removed to eliminate the crack closure effect (Borges 2020). The finite element mesh of the specimen is composed by linear hexahedral finite elements, using local refinement only near the crack tip to reduce the computational cost. Besides, the specimen thickness used in the numerical model was 0.1 mm to consider only a single layer of finite elements.

The load was applied at the upper nodes of the hole (contact zone), avoiding the modelling of the pin. Four block loading tests with various low-high and high-low sequences are carried to assess the effect of variable-amplitude on fatigue loading. Table 1 presents the sequence and the magnitude of the applied load for each load block. Each load cycle presents a triangular shape. In the case of low-high sequences, the only difference between LH1 and LH2 is the stress ratio of the first block, which is R=0.05 and R=0.36 in the LH1 and LH2, respectively. Regarding the high-low sequences, the only difference between HL1 and HL2 is the stress ratio of the second block, which is R=0.05 and R=0.36, respectively.

Table 1. Definition of the load pattern adopted in each low-high and high-low load block.

Load pattern	F_{min} (1st block) [N]	F_{max} (1st block) [N]	F_{min} (2nd block) [N]	F_{max} (2nd block) [N]
Low-High (LH1)	2.2	44.05	2.2	65
Low-High (LH2)	23.15	65	2.2	65
High-Low (HL1)	2.2	65	2.2	44.05
High-Low (HL2)	2.2	65	23.15	65

2.1. Material constitutive model

The material studied was the titanium alloy Ti6Al4V produced by selective laser melting process, which was posteriorly submitted to hot isostatic pressing for stress relieving and full densification. The elastic behavior of this titanium alloy is assumed isotropic (Hooke's law). The plastic response is described by the von Mises yield criterion, using the Swift law coupled with the Lemaître-Chaboche law to describe the isotropic and kinematic hardening, respectively. Table 2 presents the parameters of the elasto-plastic constitutive model for the titanium alloy Ti6Al4V, which were obtained fitting numerical stress-strain curves to experimental data obtained from low-cycle fatigue tests (Ferreira, 2020).

Table 2. Elasto-plastic properties of the titanium alloy Ti6Al4V.

Material	E [GPa]	ν	Y_0 [MPa]	K [MPa]	n	C_X	X_{sat} [MPa]
Ti6Al4V	115	0.33	823.5	707.1	−0.029	104.3	402.0

2.2. Crack propagation

The adopted fatigue crack growth criterion is based on cumulative plastic deformation at the crack tip (Borges, 2020). Hence, the value of cumulative plastic strain assessed numerically at the crack tip is compared with a critical value of cumulative plastic strain (parameter), defining the load cycle at which the crack propagation occurs by the nodal release. The crack increment is dictated by the mesh size (8 μm) around the crack path. Hence, the predicted FCG rate is the ratio between the crack increment (8 μm) and the number of load cycles required to induce crack extension. The calibration of the model (critical value of cumulative plastic strain) requires a single value of FCG rate measured experimentally, which is compared with the value predicted by the numerical model. Since the numerical solution for the FCG rate depends on the selected critical value of plastic strain, it is adjusted to reduce the difference between numerical and experimental FCG rate. For this titanium alloy, the calibration of the critical value of plastic strain was performed in a previous work (Ferreira, 2020), having obtained the value of 153%.

The crack closure level was defined using the contact status of the first node behind crack tip, which is given by:

$$U^* = \frac{F_{open} - F_{min}}{F_{max} - F_{min}} x100, \tag{1}$$

where F_{open} is the crack opening load. This parameter quantifies the fraction of load cycle during which the crack is closed. It is directly related with parameter U established by Elber (1970) to quantify the fraction of the load cycle over which the crack is open, i.e., $U^*=(1–U)\times100$. In order to ensure the stabilization of the residual plastic wake, the crack closure is evaluated in the load cycle immediately before the crack propagation (nodal release).

3. Results and discussion

Considering the low-high load blocks listed in Table 1, the evolution of the predicted FCG rate is presented in Fig. 1, comparing the situation with and without contact at the crack flanks. Since the FCG rate predicted by the model that neglects the contact of the crack flanks is globally higher, the relative crack length ($a–a_t$) is adopted to simplify the comparison, where a_t denotes the crack length at the transition between loading blocks.

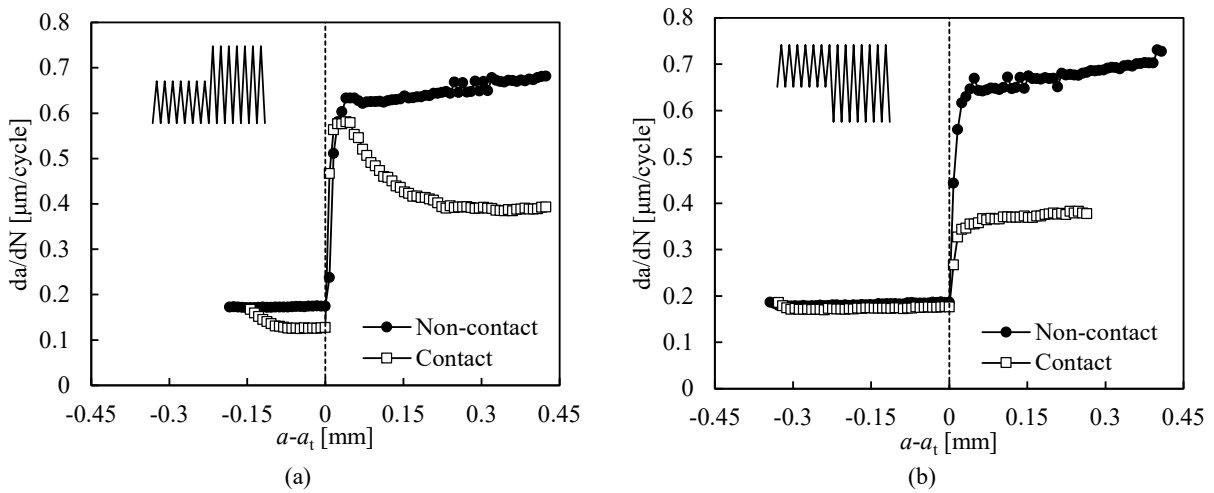

Fig. 1. Evolution of FCG rate for two different low-high load blocks, comparing the situation with and without contact of crack flanks: (a) LH1 load pattern; (b) LH2 load pattern.

Fig. 1a presents the FCG rate predicted for the LH1 load pattern (F_{min} identical in both blocks), highlighting the importance of the contact conditions in the crack flanks. The decrease of da/dN with the propagation of the crack, which is due to the formation of residual plastic wake, only occurs if the contact of the crack flanks is considered. The transient behavior observed after the transition between load blocks extends approximately 0.3 mm, obtaining da/dN=0.4 μm/cycle in the steady state regime. Without contact of crack flanks there is no transient regime and da/dN increases progressively with crack growth almost immediately after the transition. The FCG rate predicted for the LH2 load pattern (F_{max} identical in both blocks) is presented in Fig. 1b. Since the stress ratio of the first block was substantially increased from LH1 (R=0.05) to LH2 (R=0.36), the difference between contact and non-contact conditions was strongly reduced. This indicates that there is almost no crack closure in the first load block due to the relatively high stress ratio. Besides, the transient regime was shortened (0.05 mm of extend), where the predicted da/dN shows a sudden increase until achieve approximately 0.4 μm/cycle. Neglecting the contact between the crack flanks, the effect of the stress ratio vanishes and consequently the evolution of the predicted FCG rate in LH1 and LH2 load patterns is identical, as can be seen comparing Fig.1a and Fig.1b.

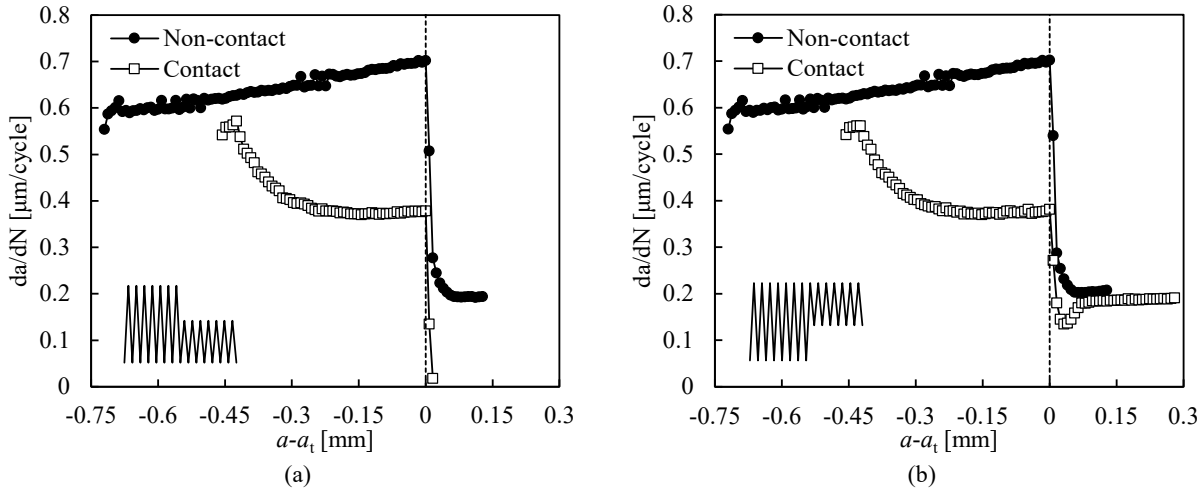

Fig. 2. Evolution of the FCG rate for two different high-low load blocks, comparing the situation with and without contact of crack flanks: (a) HL1 load pattern; (b) HL2 load pattern.

The evolution of the predicted FCG rate for both high-low load blocks listed in Table 1 is presented in Fig. 2, comparing the situation with and without contact at the crack flanks. The first load block of the load pattern HL1 and HL2 are identical. Neglecting the contact between the crack flanks, the predicted da/dN shows a gradual increase during the first load block. On the other hand, a transient behavior is observed for da/dN at the beginning of the crack propagation when the contact of the crack flanks is considered. The extension of this transient regime is about 0.3 mm, after which the da/dN reaches approximately 0.4 μm/cycle (see Fig. 2). This is the FCG rate associated to the steady state regime of the second block in the load patterns LH1 and LH2 (see Fig. 1).

Considering the HL1 load pattern (F_{min} identical in both blocks), the crack stops after the transition between loading blocks, i.e. the value of da/dN converges to zero, as shown in Fig. 2a. Nevertheless, removing the contact between the crack flanks, da/dN shows a sudden decrease until it achieves approximately 0.2 μm/cycle after 0.05 mm of crack extension. This is the FCG rate previously obtained in the first block of the load pattern LH1 and LH2, when the contact was neglected (see Fig. 1). Since the stress ratio of the second block increased from R=0.05 in HL1 to R=0.36 in HL2, the FCG rate presents a transient regime followed by a steady state evolution, as shown in Fig. 2b. Assuming the contact between the crack flanks, the predicted da/dN shows a sudden decrease in the transition between loading blocks, reaching a minimum at some point ahead of the transition. Then, da/dN increases gradually to the constant amplitude FCG rate. The extent of this transient regime is approximately 0.05 mm, either considering or not the contact between the crack flanks. The trends observed in Fig. 1 and 2 agree with the experimental results of Borrego (2002).

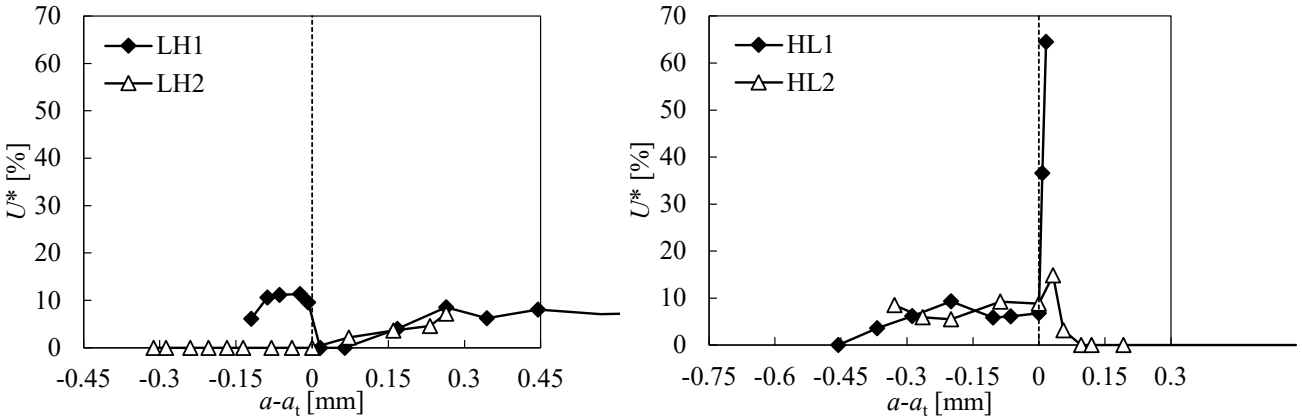

Fig. 3. Evolution of the crack closure level in different load patterns: (a) low-high load blocks; (b) high-low load blocks.

The evolution of the predicted crack closure level is presented in Fig. 3 for all load patterns studied. Regarding the crack closure phenomenon in the LH1 load pattern (Fig. 3a), the crack closure in the steady state regime of the first load block is about 11%, which vanish at the beginning of the second block. Then, it increases progressively until achieve the stable value around 7% in the second load block. Since the first block of the LH2 load pattern presents a large stress ratio (R=0.36), no crack closure was found during the entire loading block. Then, the crack closure starts to increase in the second load block since R=0.034. The crack closure predicted for the HL1 load pattern is presented in Fig. 3a. The stress ratio is relatively low in both load blocks, leading to a sudden increase of the crack closure level in the transition from low to high stress level. Since the crack closure is larger than 65% at the beginning of the second load block, the crack growth stops suddenly (see Fig. 2a). The increase of the stress ratio associated to the second load block in the HL2 load pattern yields different levels of crack closure. Indeed, the crack closure starts to increase at the beginning of the second block (achieving 15%) and then decreases until vanish, as shown in Fig. 3b. This trend in the crack closure level is in agreement with the predicted da/dN for the second load block (Fig. 2b), i.e. the FCG rate starts to decrease and then increases until achieve the steady state regime.

4. Conclusions

The effect of variable amplitude block loading on fatigue crack growth (FCG) was numerically evaluated using different low-high and high-low sequences. The influence of the contact between the crack flanks on the predicted FCG rate is highlighted by removing numerically the contact conditions. The transient behavior observed between loading blocks of different amplitude is strongly reduced or vanishes when the contact is neglected. For load blocks with high values of stress ratio, the predicted FCG rate in steady state regime is approximately the same considering or neglecting the contact of the crack flanks. On the other hand, for low values of stress ratio, the predicted FCG rate is lower when the contact of the crack flanks is considered, which is related with crack closure level.

Acknowledgements

The authors gratefully acknowledge the financial support of the Portuguese Foundation for Science and Technology (FCT) under the projects with reference PTDC/EME-EME/30592/2017 and by European Regional Development Fund (ERDF) through the Portugal 2020 program and the Centro 2020 Regional Operational Programme (CENTRO-01-0145-FEDER-031657). This research is also sponsored by the project UIDB/00285/2020.

References

ASTM E647-15, 2015. Standard Test Method for Measurement of Fatigue Crack Growth Rates. Am Soc Test Mater Annu B Stand.

Borges, M.F., Neto, D.M., Antunes, F.V., 2020. Numerical simulation of fatigue crack growth based on accumulated plastic strain. Theoretical and Applied Fracture Mechanics 108, 102676

Borges, M.F., Neto, D.M., Antunes, F.V., 2020. Revisiting Classical Issues of Fatigue Crack Growth Using a Non-Linear Approach. Materials, 13, 5544.

Borrego, L.F.P., 2002. Propagação de fendas de fadiga a amplitude de carga variável em ligas de alumínio AlMgSi. University of Coimbra, PhD Thesis.

Christensen, R.H., 1959. Fatigue crack, fatigue damage and their detection, Metal fatigue. New York: MacGraw-Hill.

Elber, W., 1970. Fatigue crack closure under cyclic tension. Engng Fracture Mechanics 2, 37-45.

Ferreira, F.F., Neto, D.M., Jesus, J.S., Prates, P.A., Antunes, F.V., 2020. Numerical Prediction of the Fatigue Crack Growth Rate in SLM Ti-6Al-4V Based on Crack Tip Plastic Strain. Metals 10, 1133.

Jones, R.E., 1973. Fatigue crack growth retardation after single-cycle peak overload in Ti–6Al–4V titanium alloy. Eng. Fract. Mech. 5, 585–604.

Menezes, L.F., Teodosiu, C., 2000. Three-dimensional numerical simulation of the deep-drawing process using solid finite elements. J. Mater. Process. Technol. 97, 100–106.

Neto, D.M., Borges, M.F., Antunes, F.V., 2021. Mechanisms of fatigue crack growth in Ti-6Al-4V alloy subjected to single overloads. Theoretical and Applied Fracture Mechanics 114, 103024.

Schijve, J., Broek, D., 1962. The result of a test program based on a gust spectrum with variable amplitude loading, Aircraft Eng. 34, 314–316.

Suresh, S., 1983. Micromechanisms of fatigue crack growth retardation following overloads, Eng. Fract. Mech. 18, 577–593.